Supporting Information

Optimum Morphology of Mixed-Olivine Mesocrystals for Li-Ion Battery

By *Kimin Park,[+] Jaewon Kim,[+] Sungun Wi,[+] Sangheon Lee, Taehyun Hwang, Jaewook Kim, Joonhyeon Kang, Joon-Phil Choi, Seunghoon Nam,[*] and Byungwoo Park[*]*

K. Park, J. Kim, Dr. S. Wi, S. Lee, T. Hwang, J. Kim, Dr. J. Kang, and Prof. B. Park

Department of Materials Science and Engineering, and Research Institute of Advanced Materials,

Seoul National University,

Seoul 08826, Korea

E-mail: byungwoo@snu.ac.kr

Dr. J.-P. Choi

Department of Mining and Materials Engineering,

McGill University,

Montreal, Quebec H3A 0C5, Canada

Dr. S. Nam

Department of Applied Mechanics, Nano Mechanical Systems Research Division,

Korea Institute of Machinery and Materials (KIMM),

Daejeon 34103, Korea

E-mail: kwek14@kimm.re.kr

Table S1. Synthetic parameters of LMFP samples and pH values measured before and after the solvothermal reaction.

Sample	Molar Ratio (Li:*TM*:PO_4)	Added Amount of HNO_3	Initial pH Value	Final pH Value
LMFP_3.0_1.6	3.0:1.0:1.0	1.6 ml	5.6	9.0
LMFP_3.0_1.8	3.0:1.0:1.0	1.8 ml	4.9	8.8
LMFP_3.0_1.9	3.0:1.0:1.0	1.9 ml	4.8	8.7
LMFP_3.0_2.0	3.0:1.0:1.0	2.0 ml	3.9	8.3
LMFP_3.0_2.4	3.0:1.0:1.0	2.4 ml	3.5	8.3
LMFP_3.3_1.6	3.3:1.0:1.1	1.6 ml	6.1	9.0
LMFP_3.3_1.8	3.3:1.0:1.1	1.8 ml	5.9	8.9
LMFP_3.3_2.0	3.3:1.0:1.1	2.0 ml	4.6	8.6
LMFP_3.3_2.4	3.3:1.0:1.1	2.4 ml	3.8	8.4
LMFP_3.3_3.0	3.3:1.0:1.1	3.0 ml	3.3	8.2
LMFP_3.6_1.7	3.6:1.0:1.2	1.7 ml	6.5	9.0
LMFP_3.6_1.8	3.6:1.0:1.2	1.8 ml	6.1	9.0
LMFP_3.6_1.9	3.6:1.0:1.2	1.9 ml	5.7	8.9
LMFP_3.6_2.5	3.6:1.0:1.2	2.5 ml	4.1	8.6
LMFP_3.6_2.9	3.6:1.0:1.2	2.9 ml	3.7	8.3
LMFP_3.9_1.7	3.9:1.0:1.3	1.7 ml	6.7	9.1
LMFP_3.9_1.8	3.9:1.0:1.3	1.8 ml	6.3	8.9
LMFP_3.9_1.9	3.9:1.0:1.3	1.9 ml	6.1	8.7
LMFP_3.9_2.8	3.9:1.0:1.3	2.8 ml	3.9	8.3
LMFP_3.9_3.2	3.9:1.0:1.3	3.2 ml	3.6	8.2

Table S2. Measured tap densities of selected LMFP samples.

	LMFP 3.0_1.6	**LMFP 3.3_1.8**	**LMFP 3.3_1.7**	**LMFP 3.6_1.8**	**LMFP 3.6_2.9**	**LMFP 3.9_1.8**
Tap Density	1.13 g cm^{-3}	1.08 g cm^{-3}	0.86 g cm^{-3}	0.93 g cm^{-3}	1.23 g cm^{-3}	1.02 g cm^{-3}

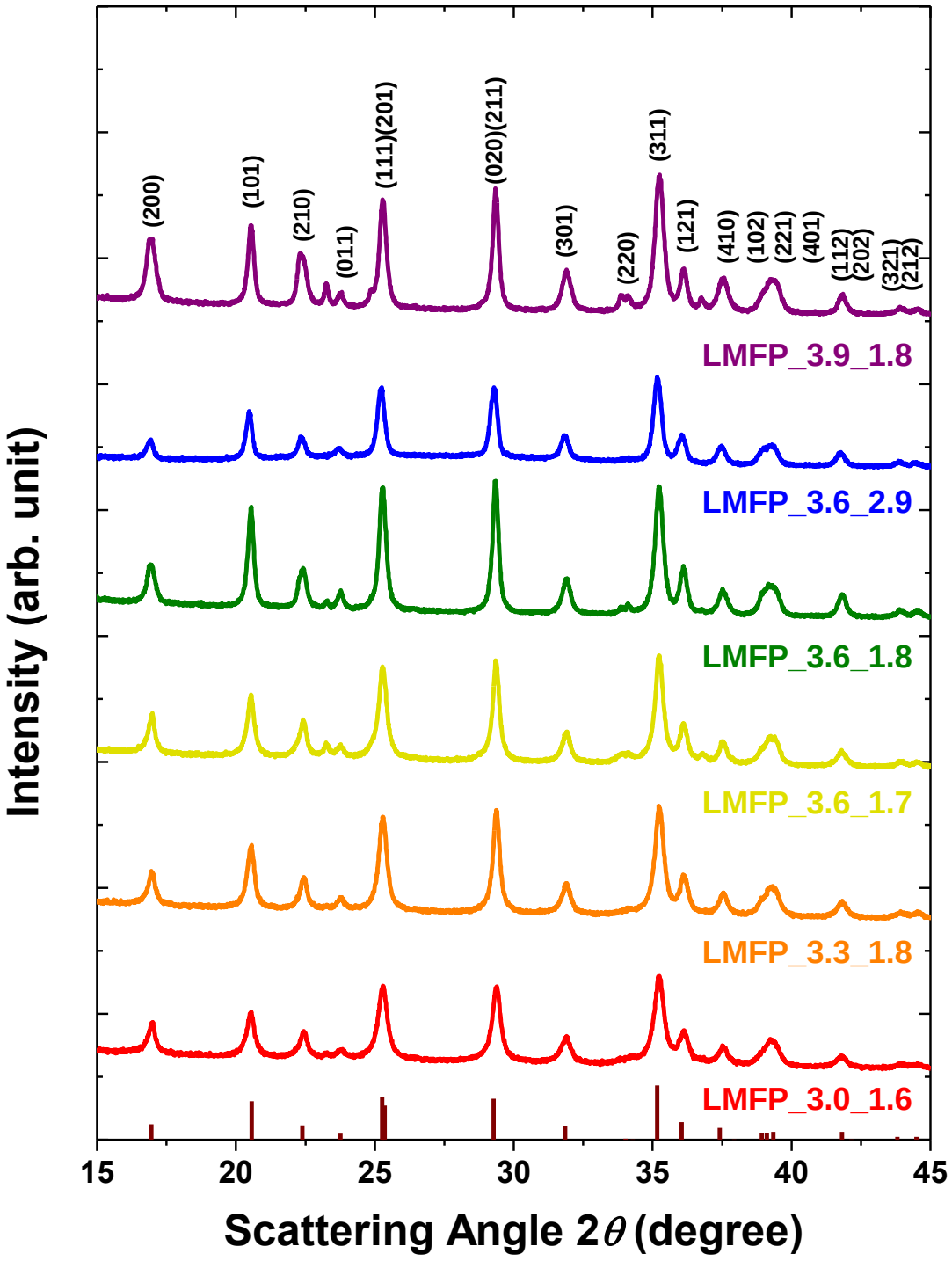

Figure S1. XRD patterns of the selected $LiMn_{0.8}Fe_{0.2}PO_4$ mesocrystal samples.

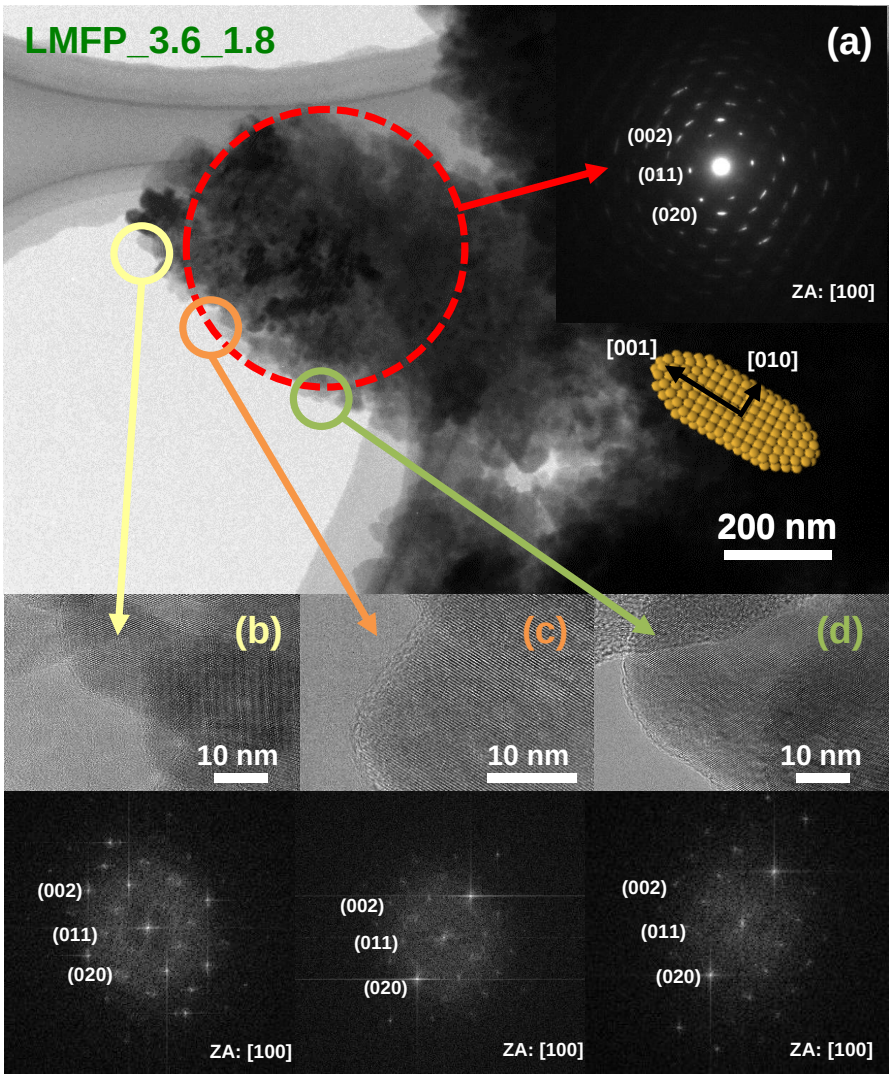

Figure S2. (a) TEM image of a $LiMn_{0.8}Fe_{0.2}PO_4$ mesocrystal (LMFP_3.6_1.8) and a selected area electron diffraction pattern of the particle along the [100] zone axis. (b-d) HRTEM images of local areas in the $LiMn_{0.8}Fe_{0.2}PO_4$ nanoparticles as marked in (a), with the corresponding fast-Fourier-transform (FFT) images along the [100] zone axis.

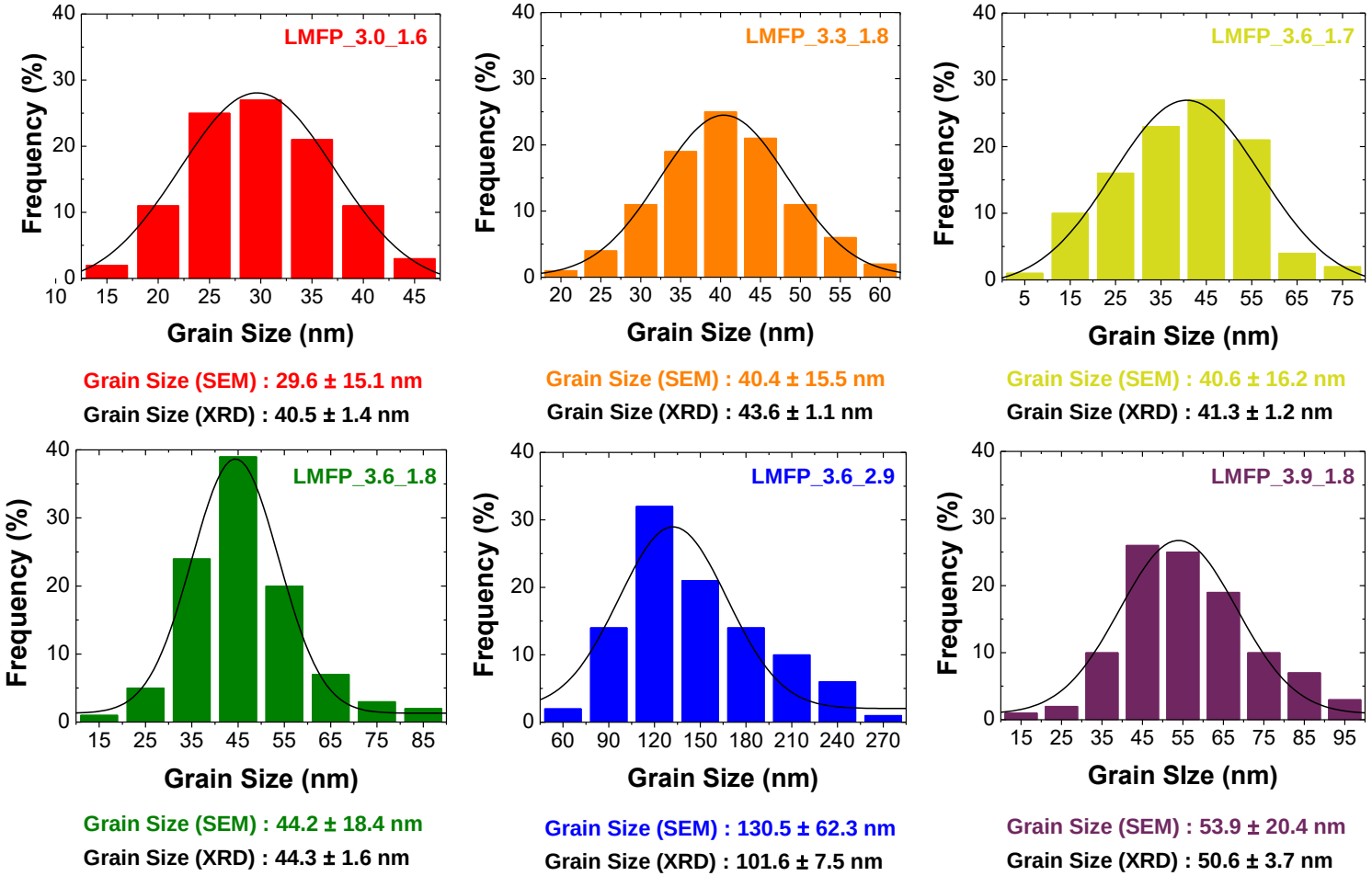

Figure S3. Primary particle size distribution of LMFP_3.0_1.6, LMFP_3.3_1.8, LMFP_3.6_1.7, LMFP_3.6_1.8, LMFP_3.6_2.9, and LMFP_3.9_1.8 by SEM. The average grain size obtained by SEM was cross-checked with the x-ray diffraction analysis.

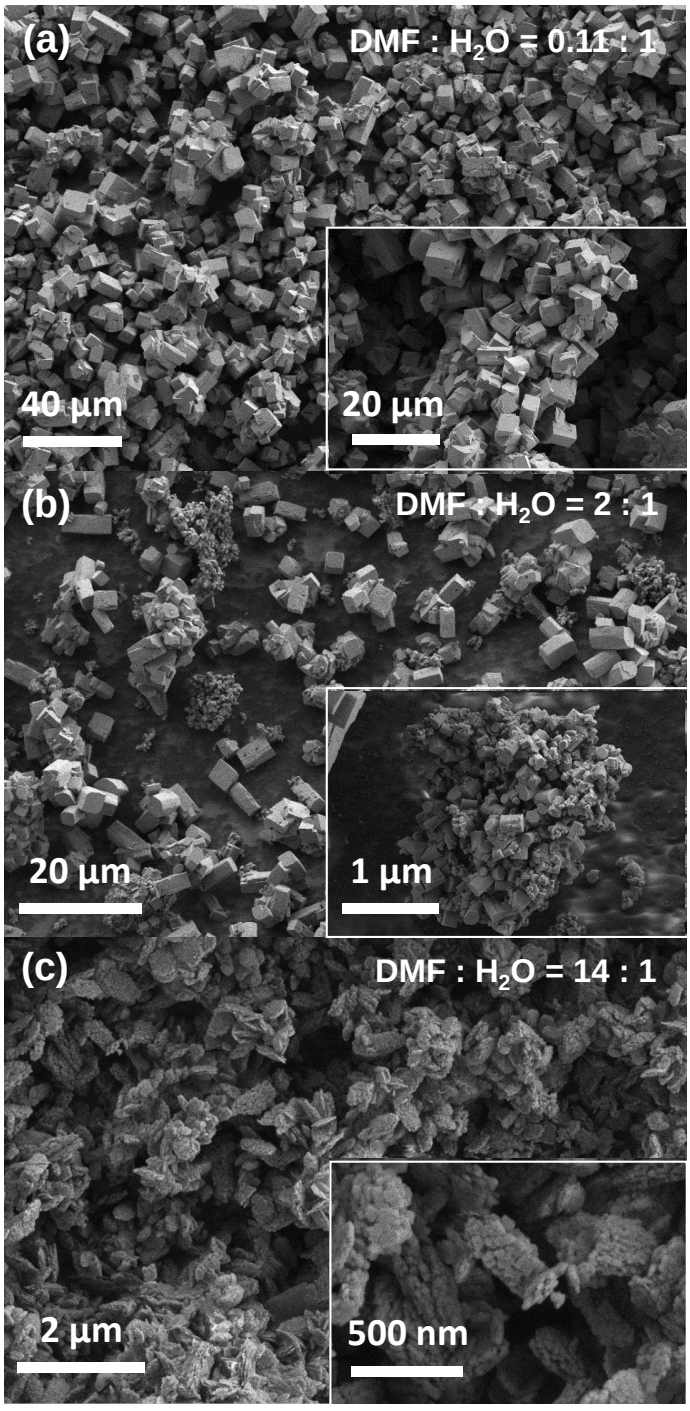

Figure S4. SEM images of $LiMn_{0.8}Fe_{0.2}PO_4$ synthesized with different solvent ratios of (a) DMF:H_2O = 0.11:1, (b) DMF:H_2O = 2:1, and (c) DMF:H_2O = 14:1.

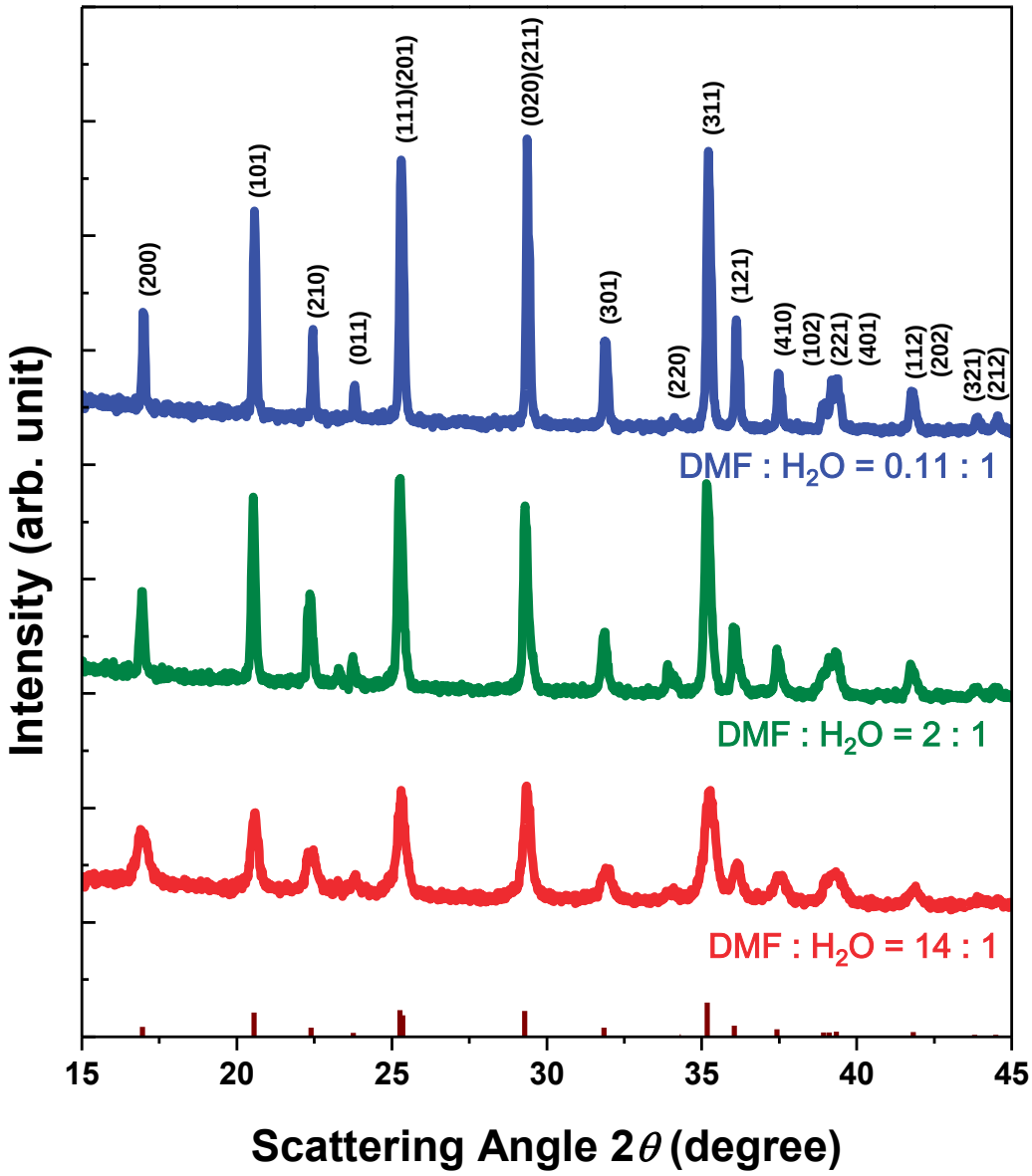

Figure S5. XRD patterns of $LiMn_{0.8}Fe_{0.2}PO_4$ synthesized with different solvent ratios of DMF:H_2O = 0.11:1, DMF:H_2O = 2:1, and DMF:H_2O = 14:1.

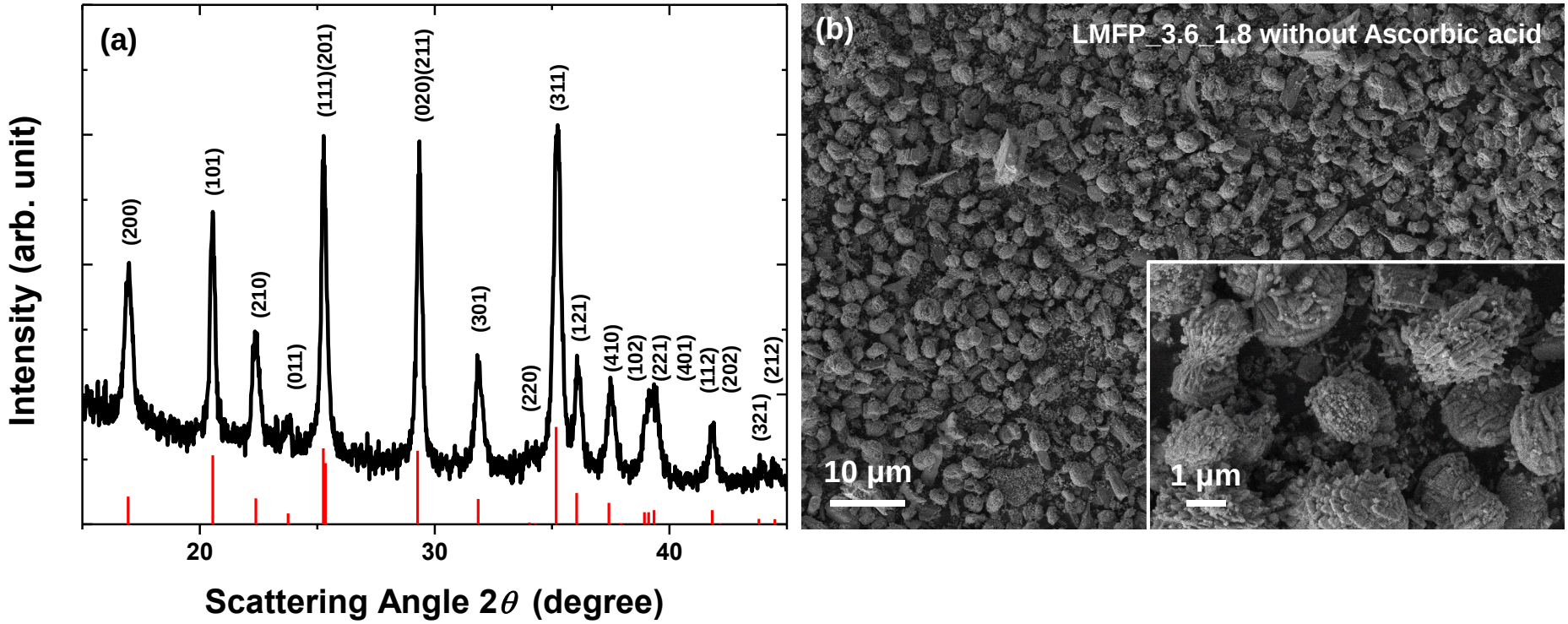

Figure S6. (a) XRD patterns and (b) SEM images of LMFP_3.6_1.8 sample synthesized without ascorbic acid.

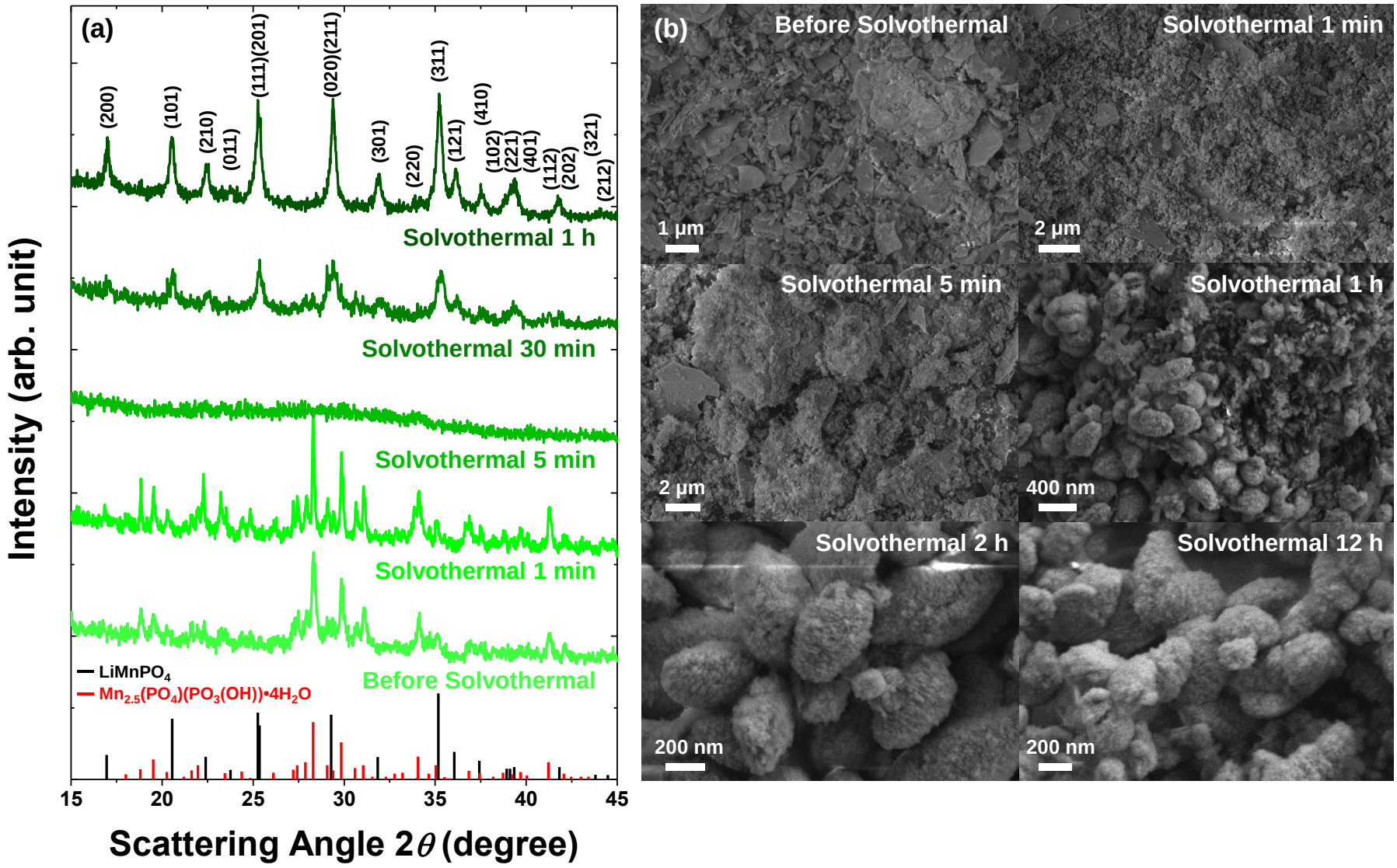

Figure S7. (a) XRD patterns and (b) SEM images of LMFP_3.6_1.7 samples obtained at different reaction times.

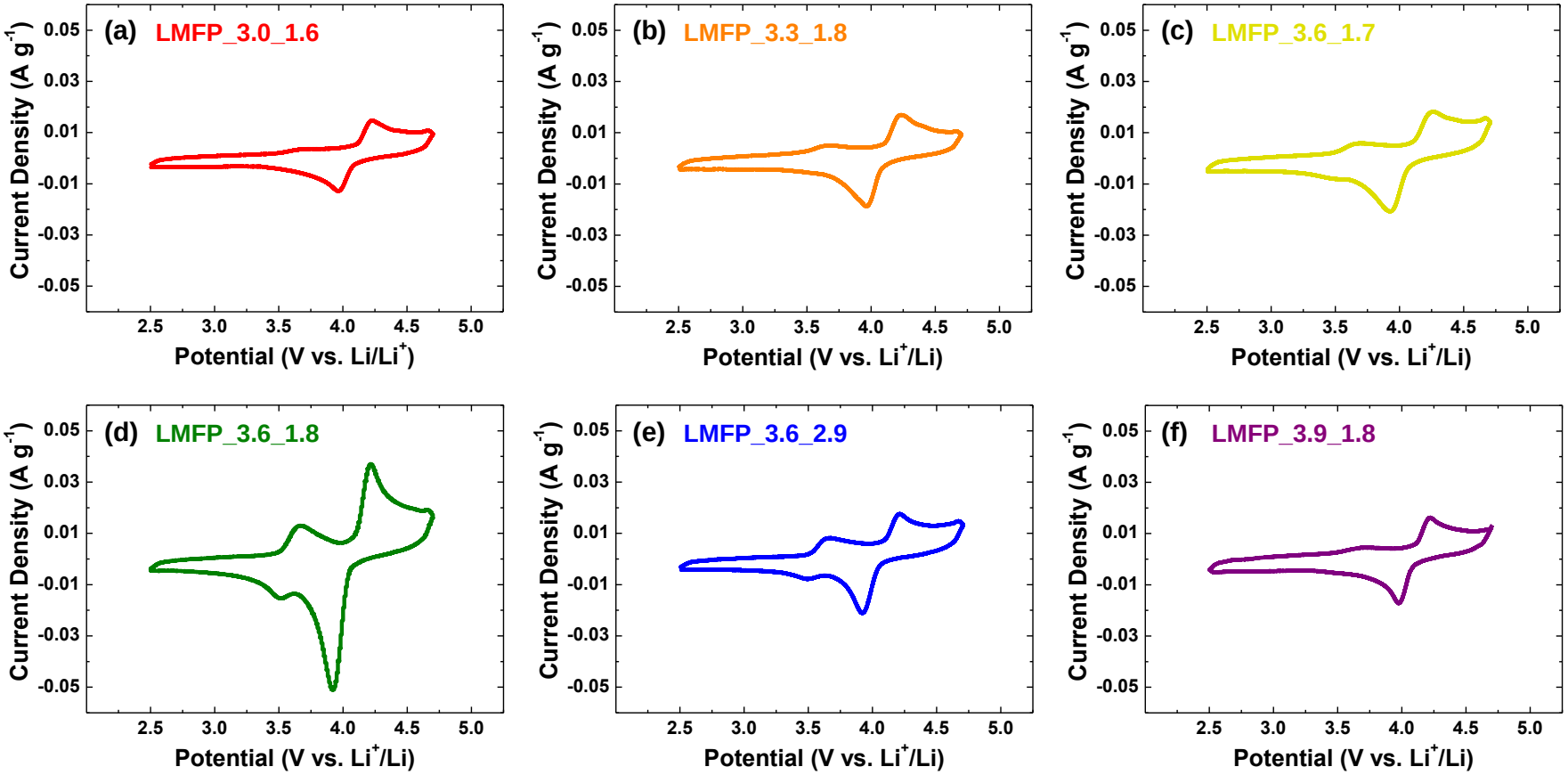

Figure S8. CV curves of (a) LMFP_3.0_1.6, (b) LMFP_3.3_1.8, (c) LMFP_3.6_1.7, (d) LMFP_3.6_1.8, (e) LMFP_3.6_2.9, and (f) LMFP_3.9_1.8 (at the scan rate of 10 mV s^{-1}).

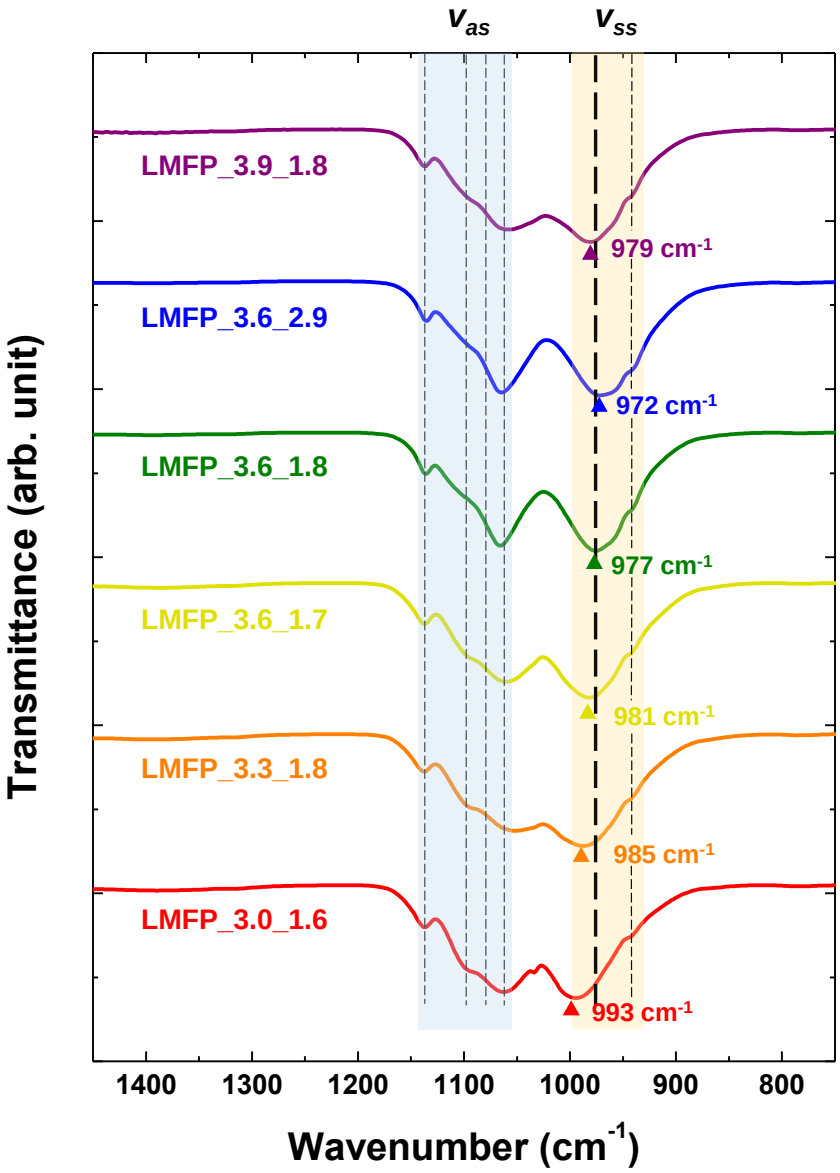

Figure S9. FTIR spectra of the selected $LiMn_{0.8}Fe_{0.2}PO_4$ mesocrystal samples. Peak positions of electrochemically optimized sample (LMFP_3.6_1.8) were marked by dashed lines. Blue and yellow regions correspond to the asymmetric and symmetric stretch modes of PO_4^{3-} tetrahedron, respectively.

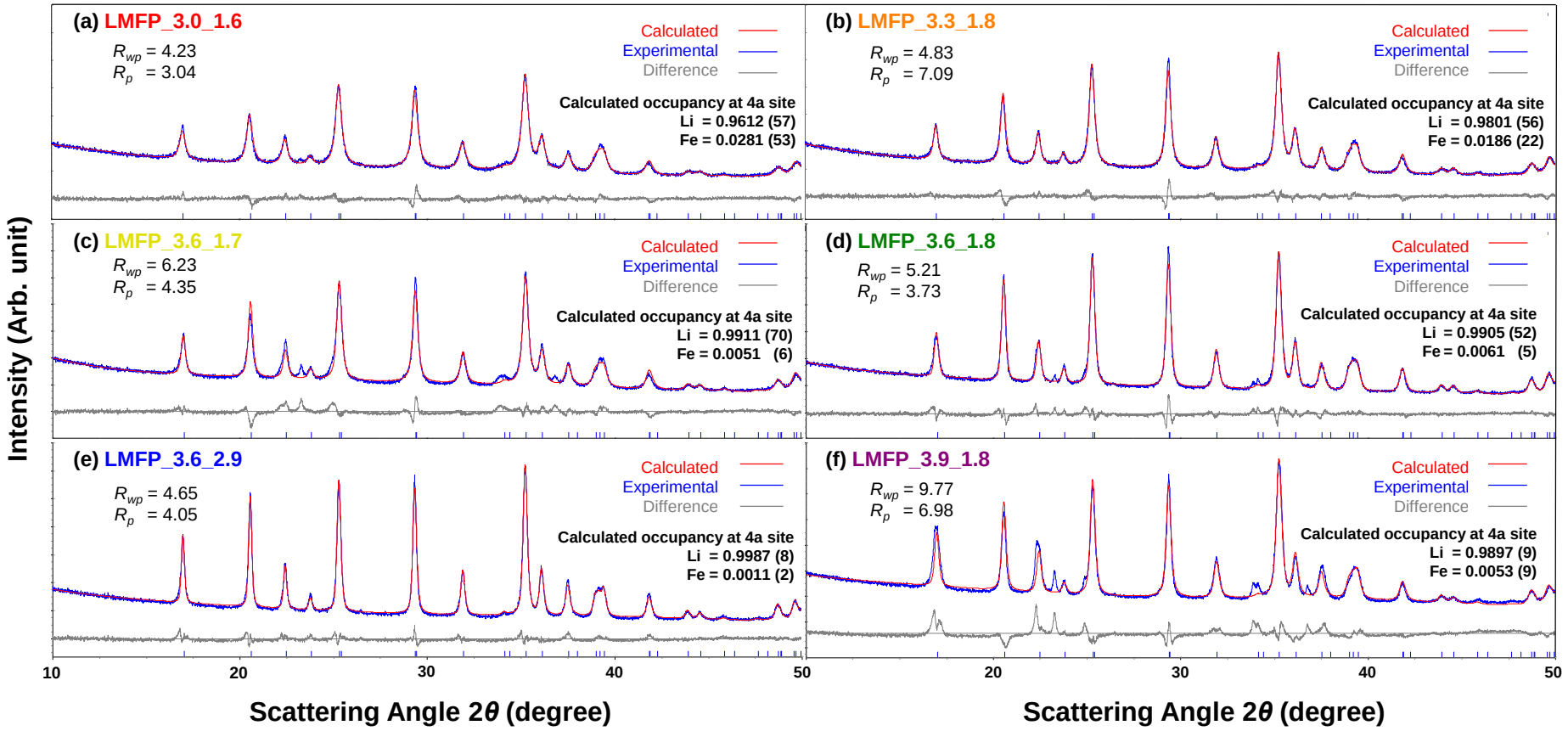

Figure S10. Rietveld refinement results of (a) LMFP_3.0_1.6, (b) LMFP_3.3_1.8, (c) LMFP_3.6_1.7, (d) LMFP_3.6_1.8, (e) LMFP_3.6 _2.9, and (f) LMFP_3.9_1.8. Occupancy values of atoms at 4*a* site (original site of Li in LMFP) were calculated for Li and Fe assuming that atomic site changes can occur only between these two atoms. The numbers in parentheses indicate estimated standard deviations of last significant digit.

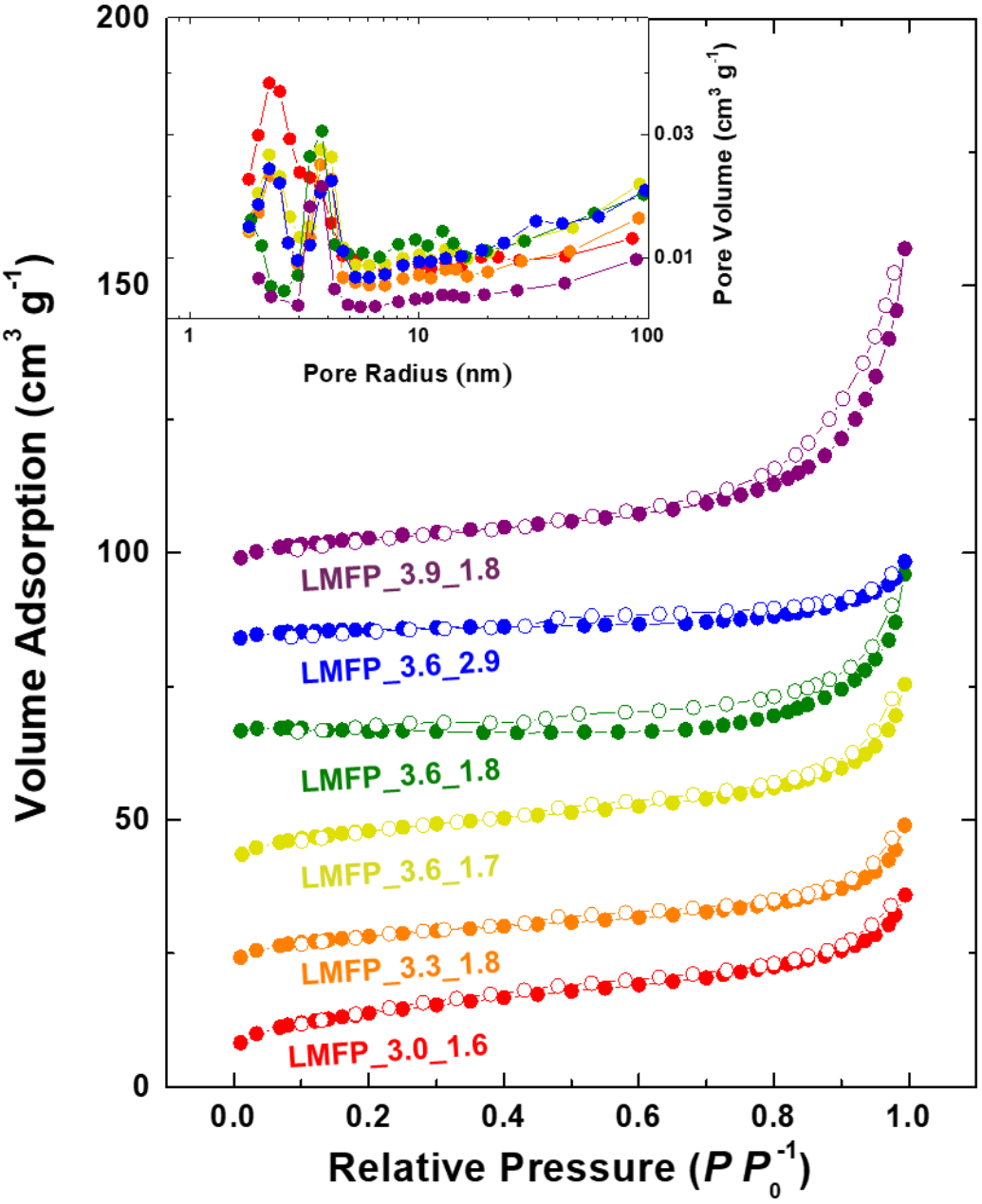

Figure S11. Nitrogen adsorption-desorption isotherms for the selected $LiMn_{0.8}Fe_{0.2}PO_4$ mesocrystals, with the pore-size distributions in the inset.

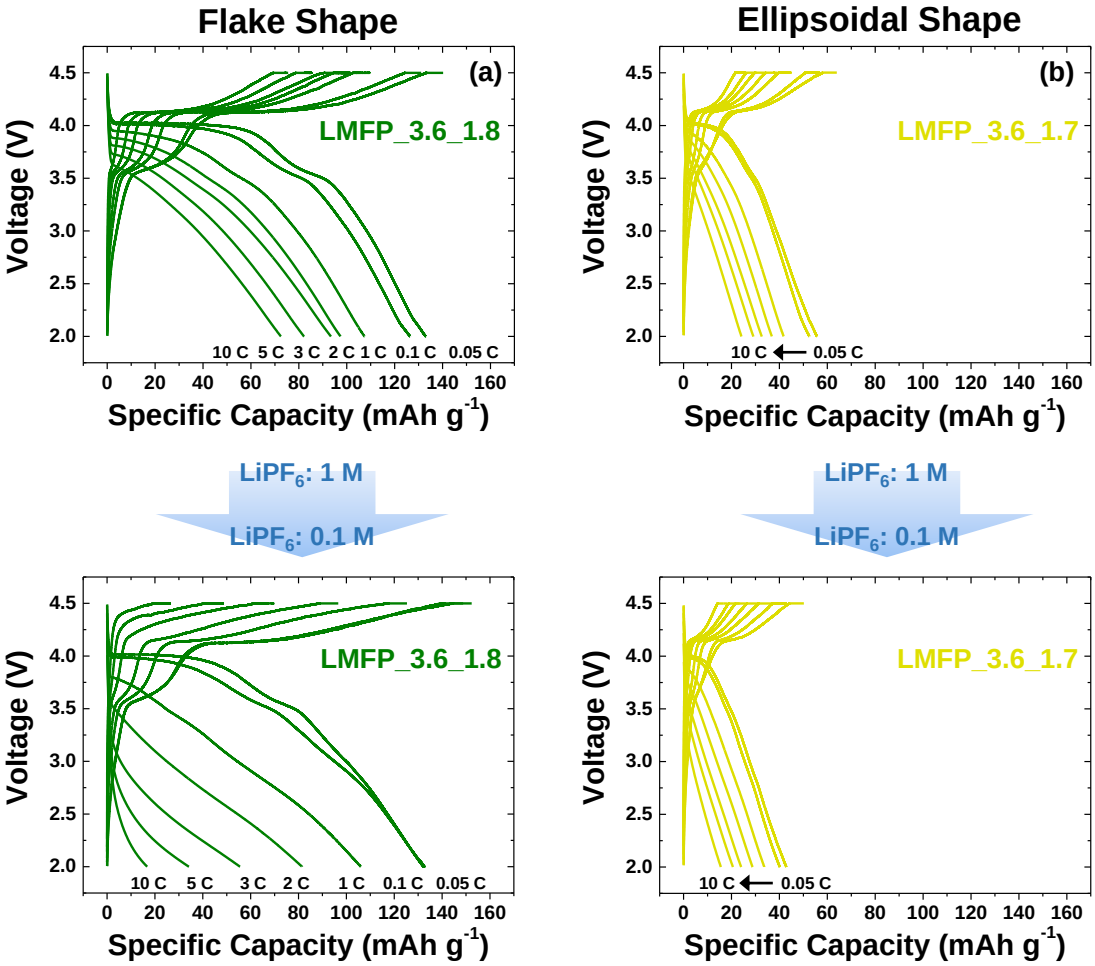

Figure S12. Comparison of the morphological effects of mesocrystals on the electrolyte permeability. The voltage profiles of two different sets of (a) LMFP_3.6_1.8 (flake-shaped), and (b) LMFP_3.6_1.7 (ellipsoidal-shaped), including two half-cell tests, each containing ordinary (1-M $LiPF_6$) or dilute (0.1-M $LiPF_6$) concentration of lithium salt.

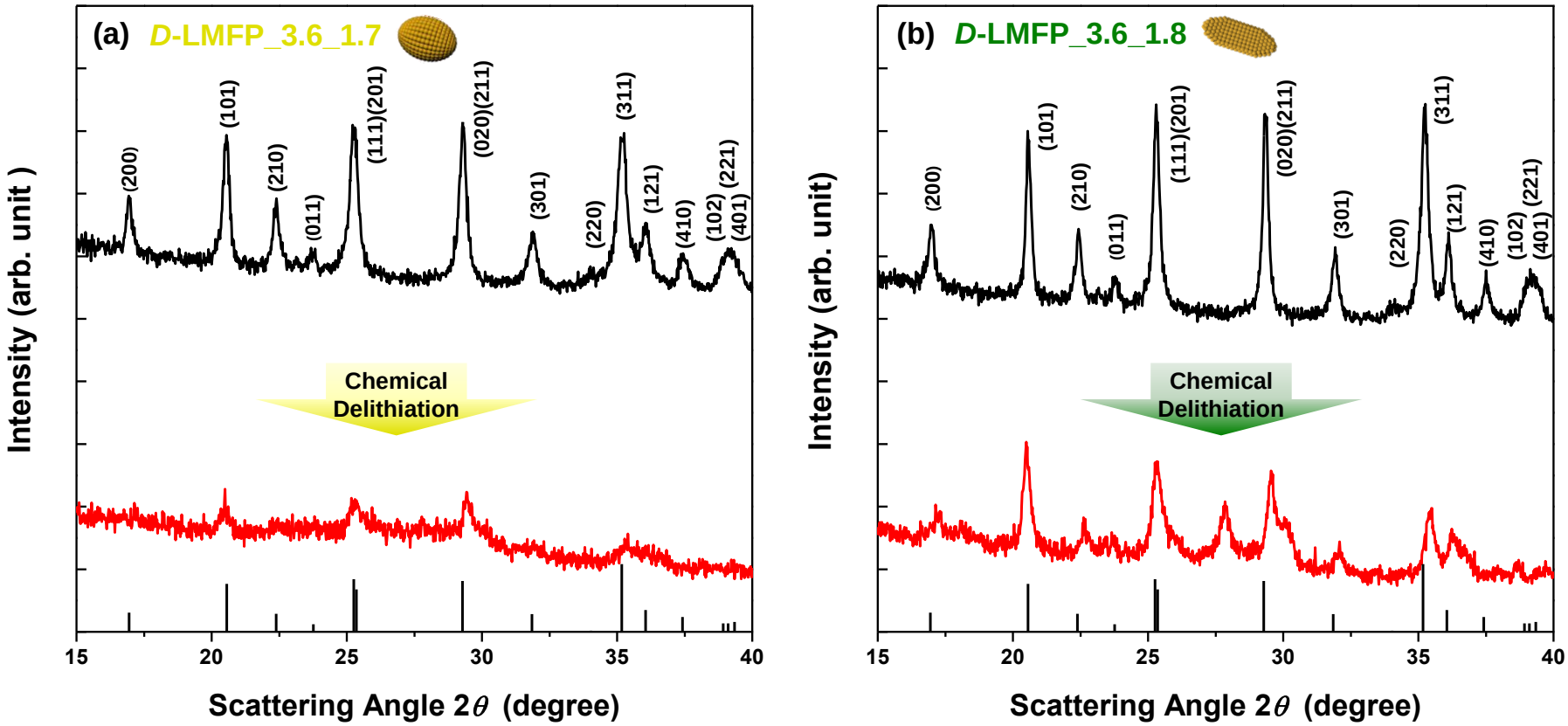

Figure S13. XRD patterns of the carbon coated $LiMn_{0.8}Fe_{0.2}PO_4$ mesocrystals and their chemically-delithiated samples (*D*-LMFP). (a) Ellipsoidal-shaped *D*-LMFP_3.6_1.7 and (b) flake-shaped *D*-LMFP_3.6_1.8.

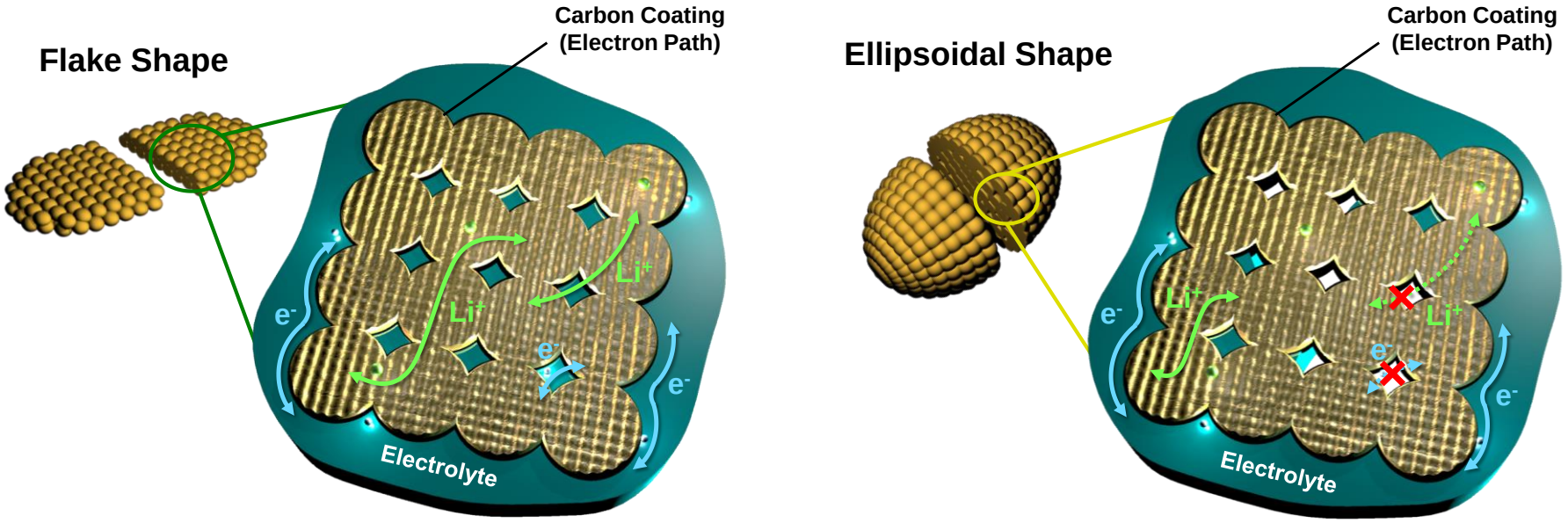

Figure S14. Schematic illustration of the morphological effects on the electrolyte permeability of the flake- and ellipsoidal-shaped $LiMn_{0.8}Fe_{0.2}PO_4$ mesocrystals.